SAE INTERNATIONAL®

Post-Impact Dynamics for Vehicles with a High Yaw Velocity

2016-01-1470
Published 04/05/2016

Nathan A. Rose, Neal Carter, and Gray Beauchamp
Kineticorp LLC

CITATION: Rose, N., Carter, N., and Beauchamp, G., "Post-Impact Dynamics for Vehicles with a High Yaw Velocity," SAE Technical Paper 2016-01-1470, 2016, doi:10.4271/2016-01-1470.

Abstract

Calculating the speed of a yawing and braked vehicle often requires an estimate of the vehicle deceleration. During a steering induced yaw, the rotational velocity of the vehicle will typically be small enough that it will not make up a significant portion of the vehicle's energy. However, when a yaw is impact induced and the resulting yaw velocity is high, the rotational component of the vehicle's kinetic energy can be significant relative to the translational component. In such cases, the rotational velocity can have a meaningful effect on the deceleration, since there is additional energy that needs dissipated and since the vehicle tires can travel a substantially different distance than the vehicle center of gravity. In addition to the effects of rotational energy on the deceleration, high yaw velocities can also cause steering angles to develop at the front tires. This too can affect the deceleration since it will influence the slip angles at the front tires. This paper explores the influence of high rotational energies and impact induced steering on the deceleration experienced by a vehicle following an impact.

Introduction

A number of sources have examined methods for determining the deceleration of a yawing and braking vehicle [Daily, 2006; Fricke, 2010; Carter, 2012]. These sources have not addressed the situation of a vehicle whose rotational kinetic energy makes up a substantial portion of its total kinetic energy. For instance, in an a 2012 paper, Carter et al. reported speed calculations for two full-scale yaw tests that utilized a 2008 Chevrolet Malibu. The yaw tests were conducted from initial speeds of approximately 48 mph and brakes were applied during portions of one of the tests. The photograph of Figure 1 depicts the vehicle in the midst of one of the tests. For performing speed calculations, Carter documented the starting and ending position of each vehicle. The test surface was surveyed and photographed, as were tire marks that were deposited during the test. A scene diagram was created from this survey data. Data acquired with a VBOX was synchronized to the tire marks. Once synchronized, the VBOX data could be examined at each vehicle location of interest. The longitudinal slip percentage and slip angle for each tire was determined at a number of positions based on the tire marks and striations [Beauchamp, 2009]. Using diagrams created from the survey data, vehicle models were aligned with the tire mark evidence. The segment lengths between positions were measured and the average vehicle sideslip angles were calculated based on the angles at the beginning and end of the segments. The steering inputs during the test were documented, and so, the tire slip angles were also determined.

Carter used three different approaches to calculate the variation of the vehicle decelerations along their trajectories. The first approach used the Bakker-Nyborg-Pacejka (BNP) tire force model [Bakker, 1987] in conjunction with the Nicolas-Comstock-Brach (NCB) combined tire force equations [Brach, 2000, 2005, 2008, 2009]. The equations for this approach are provided in Carter's paper and they are not repeated here. Carter compared the calculated speeds from the BNP/NCB model to the measured speeds from the full-scale tests and concluded that this model exhibited accurate physical behavior and yielded calculated speeds close to the measured speeds.

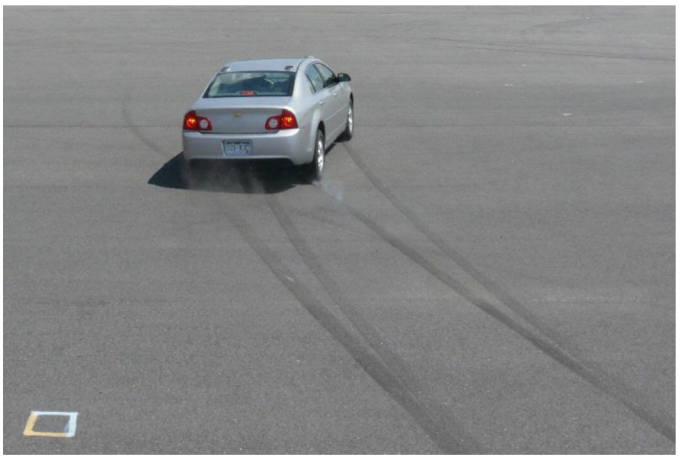

Figure 1. Photograph Taken During Test #2

The second approach discussed by Carter used a simpler equation that Martinez and Schlueter proposed for calculating the deceleration [1996]. Carter's paper demonstrated that this model exhibited

physically unrealistic behavior. Finally, the third approach discussed by Carter used Equation (1), which was attributed to the CRASH program in the 2010 edition of Traffic Crash Reconstruction by Lynn Fricke. In this equation, μ_{tire} is the effective friction force for one tire of the vehicle considering the tire slip angle (α) and braking level (f_{long}) and μ_0 is the nominal roadway coefficient of friction. The braking level f_{long} can vary between 0 and μ_0. Implementation of this equation involves calculating a μ_{tire} for each tire and then combining these into an effective friction force (μ) using a weighted averaging scheme with the static tire normal loads. This equation could also be implemented for the vehicle as a whole if the tire slip angles were not known. Carter compared the calculated speeds from the CRASH model to the measured speeds from the full-scale tests and concluded that this model exhibited accurate physical behavior and yielded calculated speeds close to the measured speeds. This model is also simpler to implement and requires fewer assumptions than the BNP/NCB model.

$$\mu_{tire} = \mu_0 \sqrt{sin^2\alpha + \left(\frac{f_{long}}{\mu_0}\right)^2 cos^2(\alpha)} \tag{1}$$

In calculating speeds at the beginning of each segment, Carter used Equation (2). This equation yielded the speed at the beginning of each segment (v_i) given the speed at the end of the segment (v_{i-1}), the calculated effective friction force (μ) for the whole vehicle, the gravitational acceleration (g), and the segment distance (Δd). Equation (2) is derived from an energy balance and it assumes, first, that rotational energy is negligible, and second, that the effective friction coefficient can be equated with the deceleration.

$$v_i = \sqrt{{v_{i-1}}^2 + 2\mu g \Delta d} \tag{2}$$

Equation (2) will be valid when the rotational kinetic energy is small in comparison to the translational kinetic energy. For the yaw tests considered by Carter in 2012, that was the case.

It will not always be the case that the rotational kinetic energy will be negligible. Impacts can induce significant yaw velocities and these yaw velocities may need to be considered when analyzing the dissipation of the post-impact energy. Essentially, some of the available friction will go toward dissipating the rotational energy, and so, less of the friction will be available for dissipating the translational energy. Equation (3) is an energy balance for the planar motion of a single vehicle that includes the kinetic energy due to the yaw velocity at the beginning (ω_i) and end of the segment (ω_{i-1}). I is the vehicle yaw moment of inertia. This equation also includes a frictional force for each tire separately. W_{ti}, is the weight on the i^{th} tire, and Δd_i is the distance traveled by the i^{th} tire during the segment. This equation recognizes the fact that, when the vehicle is spinning, each tire will travel a different distance than the vehicle center of gravity.

$$\frac{1}{2}m\left(v_i^2 - v_{i-1}^2\right) + \frac{1}{2}I\left(\omega_i^2 - \omega_{i-1}^2\right)$$

$$= \mu_{tire}(W_{t1}\Delta d_1 + W_{t2}\Delta d_2 + W_{t3}\Delta d_3 + W_{t4}\Delta d_4) \tag{3}$$

In theory, one could derive an expression for the distance traversed by each tire based on the change in center of gravity position and the change in yaw angle of the vehicle. If these expressions were substituted into Equation (3), it would then explicitly show the dependence of the energy balance on the translational and angular motion of the vehicle. In practice, though, one would be unlikely to apply such an expression. In its current form, Equation (3) is applicable, since a reconstructionist could use tire marks to actually measure the distance traveled by each tire.

Drag Factor Attenuation

In a 2008 article titled "Drag Factor Attenuation for Rotating Vehicles," Erickson stated that "even for scenarios in which all wheels/tires are locked, vehicles that undergo significant yaw rotation relative to their translational movement, exhibit effective drag factors that are well below the values exhibited during straight-line braking." The drag factor (f) referred to by Erickson is the translational deceleration of the vehicle, ignoring the spin, as defined by Equation (4). This equation, which is equivalent to Equation (2), also ignores the fact that the vehicle tires travel a different and longer distance than the center of gravity.

$$f = \frac{v_i^2 - v_{i-1}^2}{2g\Delta d_{cg}} \tag{4}$$

Substituting Equation (3) into (4) via the translational velocity term yields the following equation:

$$f = \mu_{tire}\frac{W_{t1}\Delta d_1 + W_{t2}\Delta d_2 + W_{t3}\Delta d_3 + W_{t4}\Delta d_4}{W\Delta d_{cg}} - \frac{I}{2mg\Delta d_{cg}}\left(\omega_i^2 - \omega_{i-1}^2\right) \tag{5}$$

This equation relates the underlying friction force (μ_{tire}) to the drag factor (f). When there is no spin - in straight light braking for instance - the second term of this equation goes to zero and the fraction of the first term will go to 1, since the tires will travel the same distance as the center of gravity. In this case, the drag factor will equal the effective friction coefficient. When there is spin though, the drag factor and the effective friction coefficient will not be equal. In such a case, the tires of the vehicle will travel longer distances than the center of gravity and the fraction of the first term will be greater than 1, acting to increase the drag factor. The second term also will not be zero and it will act to reduce the drag factor.

To examine the interplay of these factors and their effect on the drag factor, consider a situation similar to that Erickson analyzed with a vehicle having both translational and rotational velocity with all four wheels locked. Assume a friction coefficient of 0.75, a vehicle weight of 3,000 pounds (1,361 kg), and a yaw moment of inertia of 1,500 lbft-s^2 (2,034 kg-m^2). The authors used PC-Crash 10.1 to evaluate the drag factor for a number of different combinations of translational and rotational speed with these parameters. These simulations utilized the TM-Easy tire model. An example of this analysis is depicted in Figure 2 where the motion of 6 vehicles is depicted. The initial and rest position for each vehicle is depicted, as are the tire paths. These 6 vehicles have identical dimensions and inertial parameters and they

each have an initial speed of 20 mph. The only difference between them was their initial rotation rates. These rotation rates are indicated in Figure 2. It is evident from the motion of these 6 vehicles that increasing the rotation rate increases the distance traveled by the vehicle. It is also evident that as the rotation rate increases, so does the discrepancy between the distance traveled by the center of gravity and the distance traveled by each individual tire.

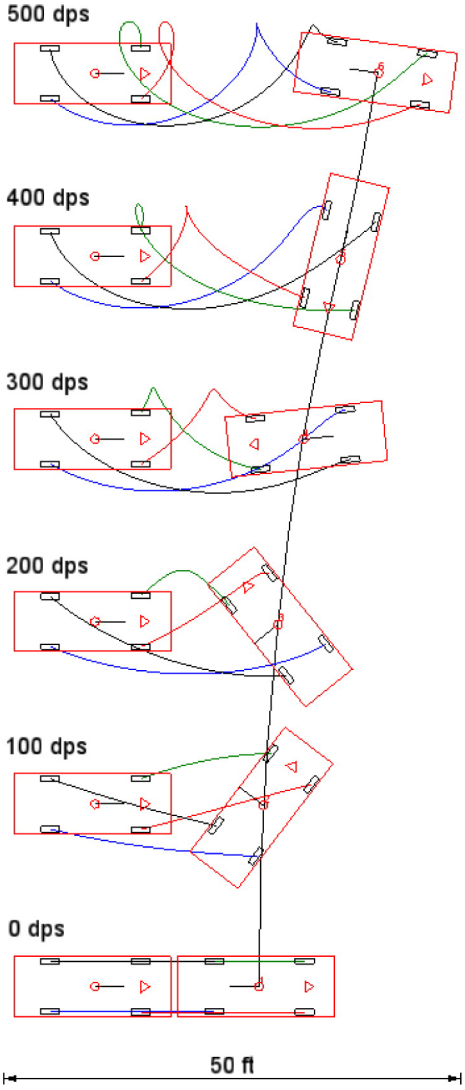

Figure 2. 6 PC-Crash Scenarios (20 mph, Varying Spin Rates)

Figure 3 plots the drag factor for 96 scenarios from PC-Crash. This graph shows that, for a situation with 4 locked wheels, as the initial yaw velocity increases, the drag factor is reduced. This effect increases in significance as the initial translational speed diminishes.

Figure 4 plots the drag factor for 96 additional scenarios from PCCrash. These simulations were identical to the previous 96 with the exception that, instead of having the wheels locked, 50% brake factors were used for each wheel. Figure 4 shows that, when the vehicle wheels are not locked, the effect of the rotational energy still increases as the translational speed decreases. It also still generally holds true that the greater the rotational velocity, the lower the drag factor - at least when there is some significant rotational velocity, even 100 degrees per second. However, the shape of the curves in Figure 4 are less consistent and predictable than those in Figure 3.

In examining the simulations, this appeared to be largely related to the orientation of the vehicle when the spin terminated. For a number of the simulations, the spin terminated in an orientation that was conducive to vehicle rollout, and so, the rotational velocity was fully dissipated at a different point in time than the translational velocity. For other simulations, the vehicle orientation was such that the translational and rotational velocity terminated at the same time. Nonetheless, Figures 3 and 4 still demonstrate that, as the rotational kinetic energy of a vehicle increases as a percentage of the total kinetic energy, the drag factor will generally decrease.

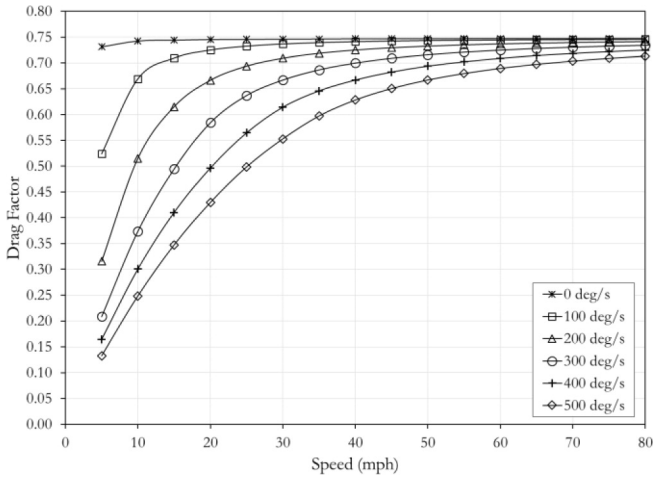

Figure 3. Dependence of Drag Factor on Speed and Spin Rate (μ = 0.75, Locked Wheels)

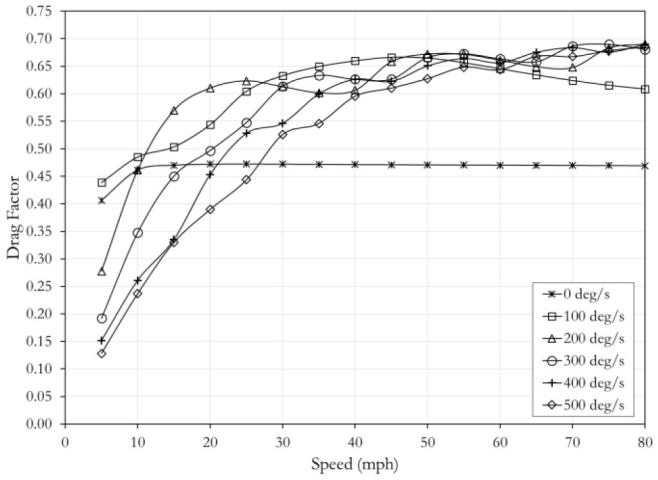

Figure 4. Dependence of Drag Factor on Speed and Spin Rate (μ = 0.75, 50% Brake Factors)

Erickson referred to the reduction in drag factor that accompanies “rapid vehicle rotation” as drag factor attenuation. He offered the following explanation for this attenuation: “When rapid vehicle

rotation is induced…the path of the rotating vehicle's tires will differ substantially from the trajectory of the center-of-gravity (cg) of the vehicle…Given that frictional drag forces acting on the vehicle are located at the tire/roadway interface and are oriented with respect to the tire trajectory (not with respect to the vehicle cg trajectory), the effective vehicle deceleration, or drag factor, can be significantly affected by vehicle yaw rotation." This statement by Erickson is generally true. However, examination of Equation (5) reveals that the effect that he describes - the discrepancy between the distance that the tires travel compared to the distance the vehicle center of gravity travels - actually acts to increase the drag factor, not decrease it. It is actually the increased kinetic energy from the rotation that acts to decrease the drag factor.

When all four wheels are locked and sliding, all of the available friction has been consumed. When a driver brakes and the vehicle is decelerating in a straight line, these frictional forces need only dissipate the translational velocity to bring the vehicle to a stop. However, if the vehicle is also spinning, the same available friction must now dissipate both translational and rotational energy. It is the additional kinetic energy due to rotation that actually explains the reduction in drag factor. The effect of the additional rotational energy holds regardless of the level of braking. The orientation of the tire forces relative to the center of gravity velocity is dealt with within the BNP/NCB and CRASH models, but once the effective coefficient of friction has been calculated, it does not change. The underlying friction force for any particular combination of slip angle and braking level remains the same, but because of the additional energy, the same underlying friction force will take a longer distance to bring the vehicle to a stop. This reduces the drag factor. That said, a more rigorous approach to dealing with "drag factor attenuation" is to calculate the effective friction coefficient using either the CRASH or BNP/NCB model - regardless of the rotation rate - and then to apply this effective friction coefficient in conjunction with Equation (3). Another rigorous approach would be to use simulation (PC-Crash or HVE, for instance) to model the vehicle motion. These software packages account for the actual tire travel distances and the effects of rotational kinetic energy using a vector mechanics approach and numerical integration.

To test the validity of Equation (3), we applied it to analyze the PCCrash scenario in which the vehicle had a translational speed of 20 mph and a rotational speed of 500 degrees per second. In this simulation, all four tires were locked and the center of gravity of the vehicle traveled approximately 31.0 feet, whereas the front left tire traveled 46.1 feet, the right front traveled 45.1 feet, and the rear tires both traveled 40.5 feet. The static wheel loads for the front tires were 743.7 pounds and for the rear tires they were 756.3 pounds. Using the 0.75 coefficient of friction (since the wheels were locked), the right side of Equation (3) predicted an energy loss of 96,879 foot-pounds. The actual initial kinetic energy was 97,200 foot-pounds. Thus, Equation (3) predicted an energy loss very close to the actual energy loss. In this instance, neglecting the rotational kinetic energy and the actual tire paths, the calculated initial speed from Equation (2) would have been 26.4 mph, 6.4 mph higher than the actual initial speed.

Impact Induced Steering

In addition to the effects of rotational energy on the drag factor, high yaw velocities can also cause steering angles to develop at the front tires. These steering angles develop, in part, because the frictional forces between the tires and ground cause the yaw rotation of the tires to lag behind the yaw rotation of the vehicle. The development of these steering angles also depends, in part, on moments generated due to the caster angle, which would cause some steering to occur even for a crash test where a significant yaw velocity did not develop.

As an illustration of impact induced steering, consider the impact-induced steering angles that develop at the front tires of a 2007 Hyundai Santa Fe SE during NHTSA Test #5832, an NCAP side impact test in which a moving deformable barrier (MDB) impacts the driver's side of the stationary Hyundai. In this test, the MDB was oriented such that it impacted the test vehicle at a 90-degree angle. However, the wheels of the MDB were crabbed at 27 degrees to the right such there was a component of the MDB velocity both into and along the test vehicle. The MDB was traveling 38.5 mph (61.94 kph). The area of direct contact began just rearward of the front wheel well, and thus, the front wheels of the test vehicle were not impacted. Figure 5 is a photograph that shows the Hyundai after this test. Examination of the post-test undercarriage photographs revealed no evidence that the steering linkages were damaged during the test.

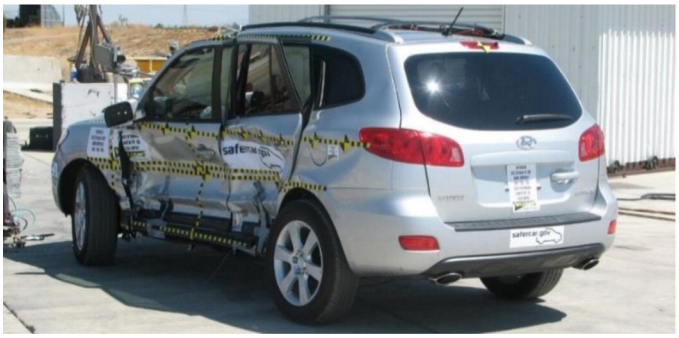

Figure 5. NHTSA Test #5832, Post Test Photograph of Hyundai Santa Fe

Figures 6, 8, 9, and 10 show select frames from several of the high speed cameras that recorded this test. The video frames in Figure 6 show an overhead view that was conducive to determining the yaw velocity of the Hyundai throughout the recorded portion of the test. The frames in Figure 6 begin at first contact (t = 0.000 seconds) and proceed in 100 millisecond intervals. The full video from this vantage point began 50 milliseconds prior to the contact and ended 500 milliseconds after the contact. There was a frame of video every millisecond. Yaw velocities determined for the Hyundai are graphed in Figure 7. As this graph shows, this impact resulted in a yaw rate of the test vehicle that peaked out at just above 80 degrees per second.

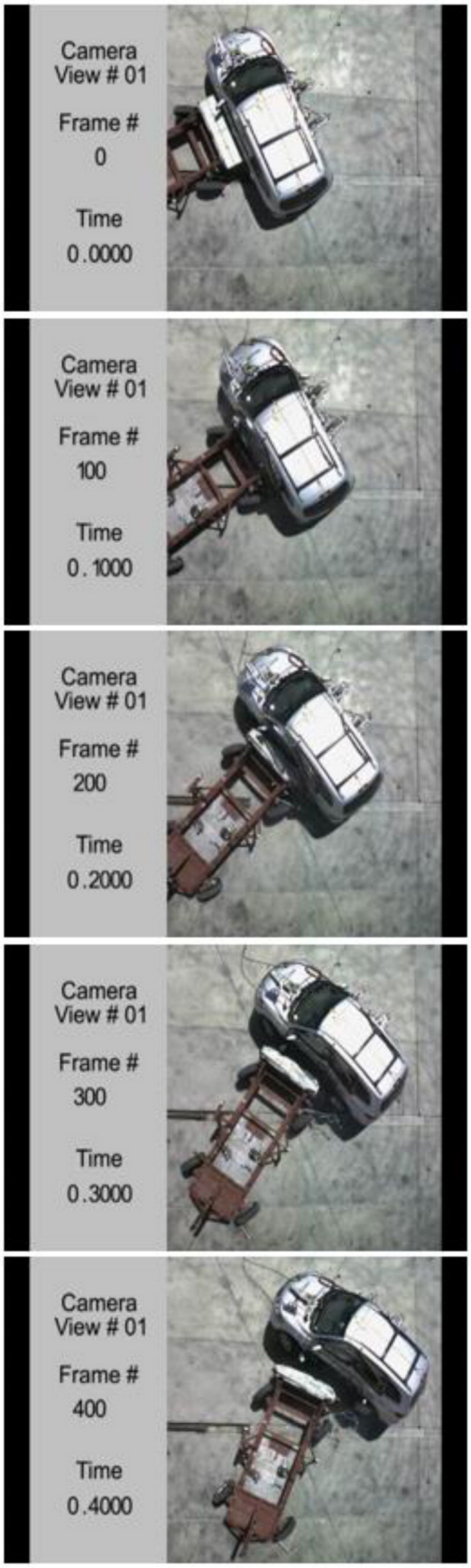

Figure 6. NHTSA Test #5832, Frames from Overhead View

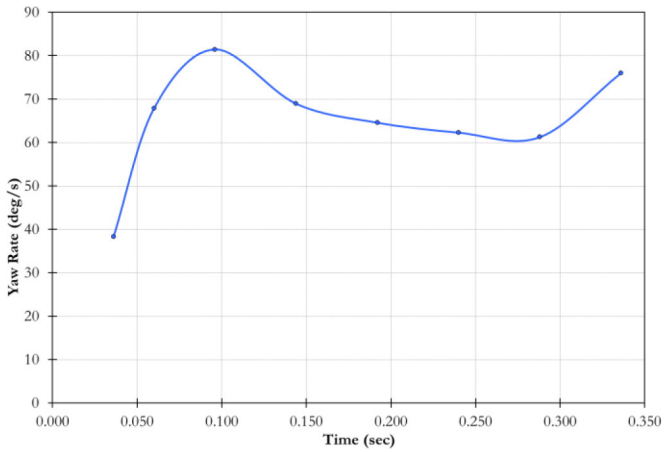

Figure 7. NHTSA Test #5832, Hyundai Yaw Rate

The video frames in Figure 8 show a ground-level, exterior view that captured the front tires of the Hyundai. This view was conducive to seeing the steering angles that developed at the front tires.

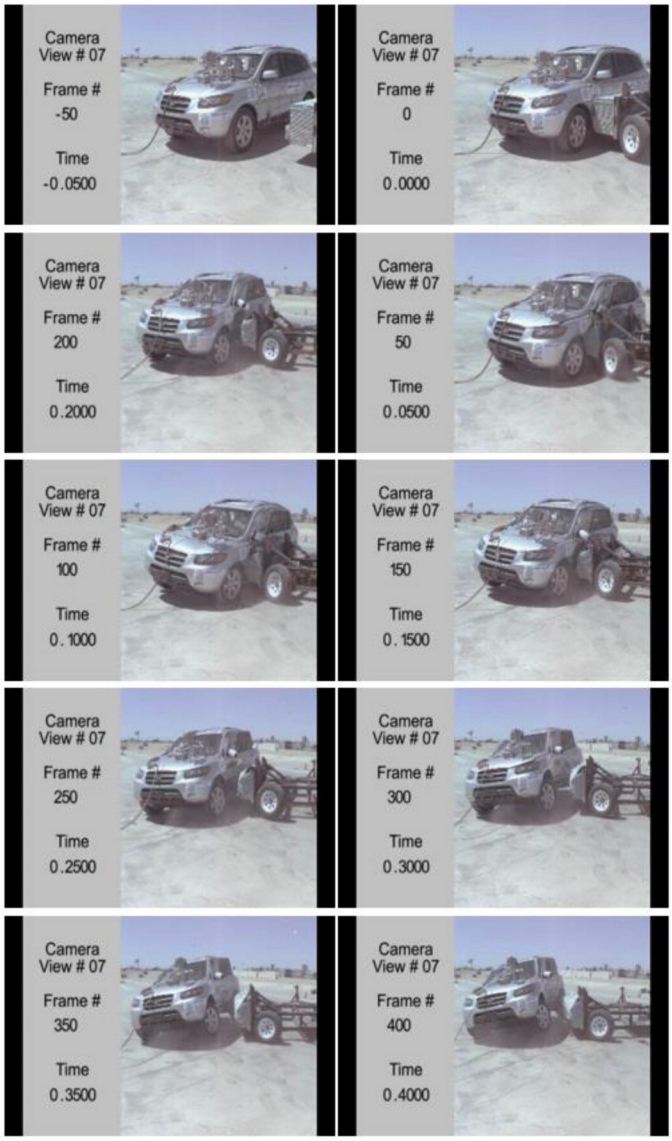

Figure 8. NHTSA Test #5832, Frames from Ground Level View

The frames in Figure 8 begin 50 milliseconds prior to first contact and proceed in 50 millisecond intervals. The full video from this vantage point began 50 milliseconds prior to the contact and ended 494 milliseconds after the contact. There was a frame of video every millisecond. From this vantage point, it is evident that a considerable rightward steering input builds up for the Hyundai during this test.

The video frames in Figures 9 and 10 show views of the steering wheel that were conducive to quantifying the steering angles that develop during the test based on how much and when the steering wheel rotates during the test. These views also show that the driver's side curtain airbags of the Hyundai deployed during the impact. There was no frontal airbag deployment during the impact. The frames in Figures 9 and 10 begin at first contact between the MDB and the Hyundai (t = 0.000 seconds) and proceed in 32 millisecond intervals through a time of 288 milliseconds. The full videos from these vantage points began 10 milliseconds prior to the contact and ended about 300 milliseconds after the contact. There was a frame of video every millisecond.

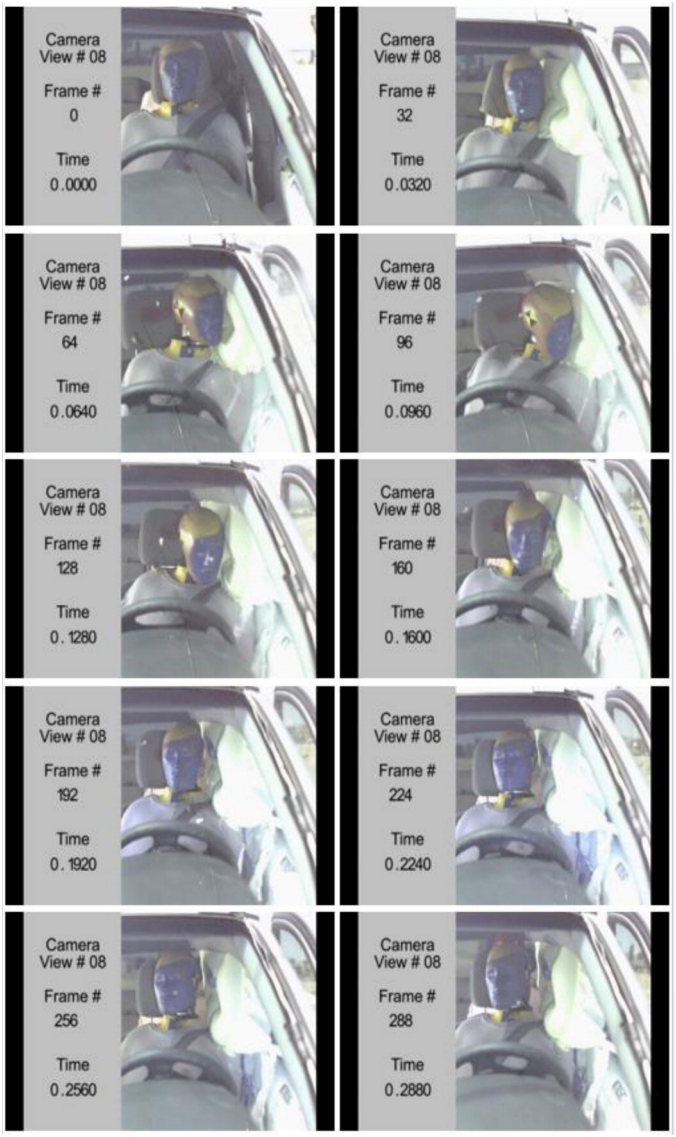

Figure 9. NHTSA Test #5832, Frames from Rear Facing View Showing Steering Wheel

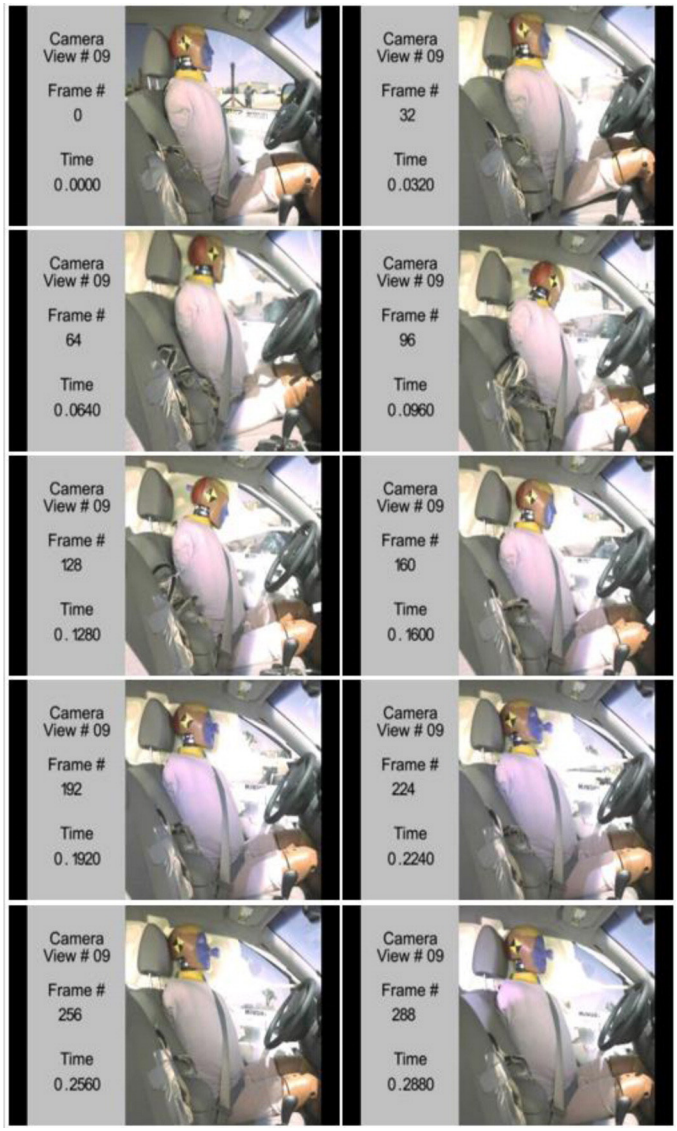

Figure 10. NHTSA Test #5832, Frames from Interior View Showing Steering Wheel

During and after the impact, the front wheels of the Hyundai develop steering when the frictional forces between the front tires and the ground caused the yaw rotation of the front tires to lag behind the yaw rotation of the rest of the vehicle during impact-induced vehicle yawing. Steering wheel angles determined for the Hyundai from the videos of Figures 9 and 10 are graphed in Figure 11. As this graph shows, this impact resulted in a steering wheel angle of approximately 260 degrees building up during the test.

Similar analysis was conducted for 9 additional NHTSA side impact tests, all of which had a nominal impact speed for the MDB of 38.5 mph (62 kph). The results of this analysis, namely the maximum clockwise steering wheel angle achieved in each test - are listed in Table 1. Two observations are apparent from this data. First, impact induced steering occurred in all of the tests, but the magnitude varied. Second, in most of the tests, the steering wheel angle was still increasing when the interior video depicting the steering wheel ended. Thus, the actual maximum steering angles would be higher than what is reported in Table 1. For all ten of the tests considered here, side impact airbags deployed, but frontal airbags did not. The

degree to which a frontal airbag deployment could affect the magnitude of impact induced steering has, therefore, not been explored in this study.

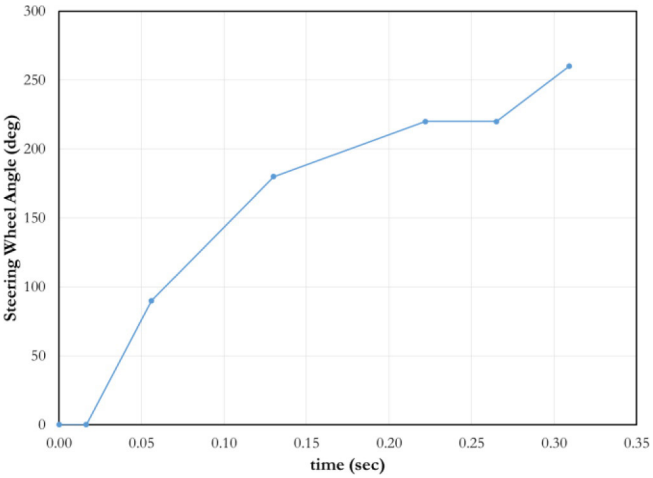

Figure 11. NHTSA Test #5832, Steering Wheel Angles

Table 1. Impact Induced Steering in Additional Side Impact Crash Tests (*Steering still increasing when video ends.)

NHTSA Test #	Test Vehicle	Maximum Steering Wheel Angle (deg)	Time of Maximum Steering Angle (sec)
5832	2007 Hyundai Santa Fe	260	0.310
5673	2006 Chevrolet Monte Carlo	100	0.310
5682	2006 Chevy Cobalt	85	0.310*
5749	2007 Lexus ES	70	0.310*
5829	2006 Ford Freestyle	95	0.310*
5831	2006 Ford 500	85	0.310*
5257	2005 Ford Mustang	185	0.300
5568	2006 Honda Civic	170	0.310*
5748	2006 Toyota RAV 4	65	0.310*
5696	2006 Kia Rio	95	0.250

Both impact-induced yawing and vehicle deformation can cause steering angles to develop during real-world crashes. In addition to steering induced by the frictional forces in the tire contact patch, as described above, the front wheels may also develop steering angles due to side structure deformation if components interact with the vehicle's instrument panel or steering wheel. This deformation-induced steering would occur during the period of contact between vehicles. These steering angles play a part in determining the motion of a vehicle following an impact. This being the case, in some instances, their inclusion in speed calculations or simulations may improve the accuracy. This assumes that, because of the impact forces, the driver is no longer holding or controlling the steering wheel. The validity of this assumption will, of course, depend on the severity of the impact. The more severe the impact, the more likely this assumption is to be true. Fortunately, the case where this assumption is most likely to be true are also the cases where the analysis is most likely to benefit from consideration of impact-induced steering.

Effects of Impact Induced Steering in Simulation

To illustrate the potential effects of impact induced steering, a simulation was generated using PC-Crash Version 10.1 [Steffan, 1996; Cliff, 1996, 2001, 2004; Bailey, 2000]. This simulation involved the front of a Ford Expedition striking the driver's side rear of a Ford E250 van. The image of Figure 12 shows the vehicle positions from this simulation for both impact and rest. The Expedition is represented with red and the E250 is represented with blue. The tire marks generated by the simulation are also shown in this figure. Canadian vehicle specifications were utilized for the vehicle weights and dimensions and PC-Crash default values were used for the moments of inertia and suspension stiffness. The center of gravity height for each vehicle was set at 39% of its total height [Allen, 2003]. The TM-Easy tire model was used, with its default parameters. A coefficient of friction of 0.75 was used for the simulation. The Expedition was traveling 55 mph and the E250 was traveling 25 mph. The coefficient of restitution was set at 0.1 and the impulse ratio at 0.6.

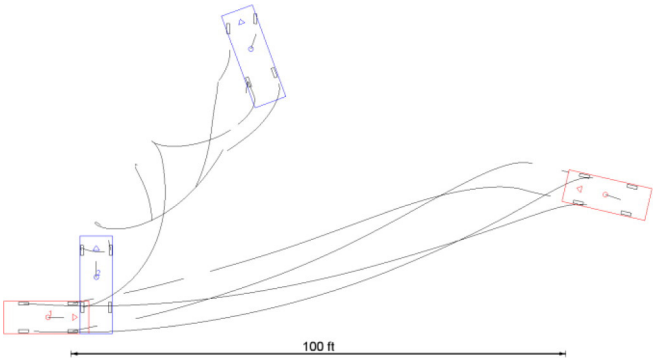

Figure 12. Baseline PC-Crash Simulation with Impact Induced Steering Included for the Northbound Ford E250

Following the impact, the front wheels of the Expedition were assumed to be mechanically impinged to some degree and brake factors of 50% were used for these front wheels. Engine drag was assumed to be present for the rear wheels of this vehicle and brake factors of 5% were used for these wheel positions. The driver's side rear wheel of the E250 was directly impacted and this wheel position was assumed to be entirely mechanically impinged following the impact. The brake factor for this wheel was set at 100%. The brake factor for the passenger's side rear wheel was set at 25% and the front wheel positions were set at 1% to represent some small level of rolling resistance. For this illustration, impact induced steering was included for the E250. This steering input was programmed in the PC-Crash sequences such that 360 degrees of clockwise (rightward) steering wheel rotation would occur during the first 250 milliseconds following the impact. This steering input was then maintained for the remainder of the simulation. The magnitude of this steer input was chosen to be higher than those listed in Table 1 because the post-impact yaw velocity of the E250 was greater than the post impact yaw velocity seen in any of the NHTSA tests. These simulation parameters resulted in the Expedition traveling 117 feet after impact and rotating counterclockwise approximately 167 degrees. The post-impact deceleration for the Expedition was 0.530g. The E250 traveled 58 feet and rotated counterclockwise approximately 380 degrees. The post-impact deceleration for the E250 was 0.356g. The peak yaw velocities of approximately 105 degrees per second for the Expedition and of approximately 350 degrees per second for the E250 occurred immediately following the impact. For the Expedition, the post-impact kinetic energy due to translation was 105,699 foot-pounds, whereas the post-impact kinetic energy due to rotation was 86,098 foot-pounds. Thus, the rotational kinetic energy made up approximately 45% of the post-impact kinetic energy for this vehicle. Given these kinetic energies, the drag factor would be attenuated to about 55% of the effective friction coefficient.

After running this baseline simulation, the rest positions and tire marks from it were treated as if they were evidence from a real world crash. The rest positions and tire marks were traced to act as an evidence diagram for subsequent simulations. In the first of these subsequent simulations, the impact induced steering was removed and the simulation was rerun. No other changes were made to the simulation. The results of this second simulation are shown in Figure 13. In this figure, the rest positions and tire marks from the baseline simulation are shown in black. The rest position and tire marks for the Expedition in this new simulation are shown in red and the rest position and tire marks for the E250 are shown in blue. Without the contribution of the impact induced steering, the E250 rotated 423 degrees, 43 more than in the baseline simulation. The vehicle center of gravity again traveled 58 feet, but came to rest in a different location than in the baseline simulation. The Expedition again traveled 117 feet after impact and rotated counterclockwise approximately 167 degrees.

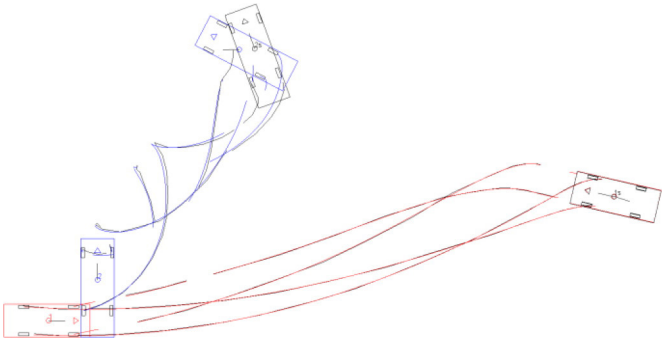

Figure 13. PC-Crash Simulation with Impact Induced Steering Removed

Next, the PC-Crash collision optimizer was used in an attempt to match the tire marks and rest positions of the vehicles without the use of impact induced steering. The optimization routine was set to consider the rest positions of both vehicles and three intermediate positions of the E250. The optimizer was allowed to vary the vehicle impact speeds, the impact location and height, the coefficient of restitution, and the inter-vehicular friction coefficient (impulse ratio). The optimization routine was run several times - until subsequent runs no longer improved the results - and it was started with the vehicle speeds far from the actual speeds of the baseline simulation.

The vehicle trajectory results are shown in Figure 14. Again, in this figure, the rest positions and tire marks from the baseline simulation are shown in black, the rest position and tire marks for the Expedition in the optimized simulation are shown in red, and the rest position and tire marks for the E250 are shown in blue. In this figure, the tire marks deposited by each vehicle during the optimized simulation are depicted with the same color as the vehicle that deposited them. The tire marks from the baseline simulation are shown in black. The optimizer error for this simulation was 2.4%. The match with the rest positions was acceptable, though certainly not perfect. The optimized solution had a coefficient of restitution of 0.1 and an impulse ratio of 0.81. This simulation resulted in impact speeds for the vehicles of 54.5 mph (0.5 mph low) and 23.5 mph (1.5 mph low). The Expedition traveled 114 feet after impact and rotated counterclockwise approximately 167 degrees. The post-impact deceleration for the Expedition was 0.532g. The E250 traveled 60 feet and rotated counterclockwise approximately 382 degrees. The post-impact deceleration for the E250 was 0.311g, 13% lower than in the baseline simulation. The peak yaw velocities of approximately 104 degrees per second for the Expedition and of approximately 343 degrees per second for the E250 occurred immediately following the impact.

An additional simulation was optimized with half the amount of impact induced steering as what was present in the baseline simulation (180 degrees at the steering wheel building up over 0.25 seconds). The optimization routine was again set to consider the rest positions of both vehicles and three intermediate positions of the E250. The optimizer was again allowed to vary the vehicle impact speeds, the impact location and height, the coefficient of restitution, and the inter-vehicular friction coefficient (impulse ratio). The optimization routine was again run repeatedly until subsequent runs no longer improved the results. The optimization was started with the vehicle speeds far from the actual speeds of the baseline simulation.

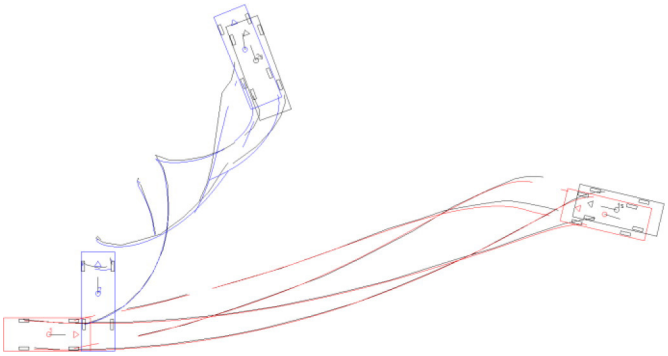

Figure 14. Optimized PC-Crash Simulation without Impact Induced Steering (Optimizer Error = 2.4%)

The vehicle trajectory results for this fourth simulation are shown in Figure 15. The rest positions and tire marks from the baseline simulation are shown in black, the rest position and tire marks for the Expedition in the optimized simulation are shown in red, and the rest position and tire marks for the E250 are shown in blue. Again in this figure, the tire marks deposited by each vehicle during the optimized simulation are depicted with the same color as the vehicle that deposited them. The tire marks from the baseline simulation are shown in black. The optimizer error for this simulation was 1.1%. The match with the rest positions was better than the previous simulation. The optimized solution had a coefficient of restitution of 0.1 and an impulse ratio of 0.6. This simulation resulted in impact speeds for the vehicles of 54.5 mph (0.5 mph low) and 24.5 mph (0.5 mph low).

This series of simulations illustrates that impact induced steering can affect simulation accuracy. The error in the simulation that ignored impact induced steering was small and the importance of including this factor in a simulation should not be over-emphasized. Nonetheless, some simulations will be improved with the inclusion of impact induced steering. The crash scenario considered here resulted in a significant yaw velocity of 350 degrees per second for the impacted vehicle. It is this type of circumstance where the inclusion of impact induced steering can be expected to improve the simulation. Typically, the actual magnitude of the impact induced steering will not be known and the analyst will likely be using the magnitude and timing of the steering as one variable that can be manually varied to obtain a good fit with the evidence.

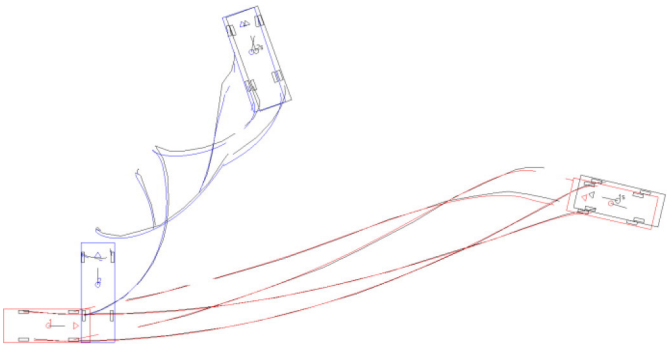

Figure 15. Optimized PC-Crash Simulation with Half the Impact Induced Steering of the Baseline Simulation (Optimizer Error = 1.1%)

Summary/Conclusions

Calculating the speed of a yawing and braked vehicle often requires an estimate of the vehicle deceleration. When a yaw is impact induced and the resulting yaw velocity is high, the rotational component of the vehicle's kinetic energy can be significant relative to the translational component. In such cases, the rotational velocity can have a meaningful effect on the deceleration. For the same calculated effective friction coefficient (determined based on the BNP/NCB or CRASH models), a vehicle with significant yaw velocity will decelerate at a lower rate than a vehicle that does not. This is because the yaw velocity is additional energy that the frictional forces must dissipate. The distance travelled by the tires of the vehicle will also differ from the distance travelled by the vehicle center of gravity. The analyst can consider these factors with Equation (3) or with simulation.

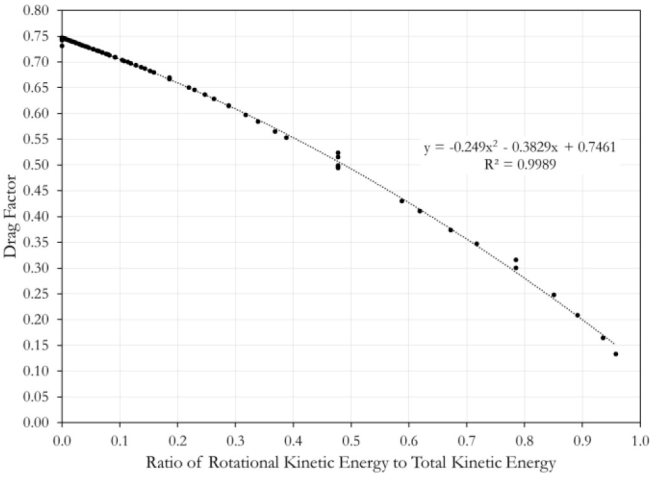

Figure 16. Dependence of Drag Factor on Rotational Kinetic Energy (μ = 0.75, Locked Wheels)

The question remains, though, what constitutes a "significant" or "high" yaw velocity that needs to be considered in the speed calculations? To answer this question, consider Figure 16, a graph that contains the same PC-Crash simulation scenarios as Figure 3 - the locked wheel scenarios. In this case, though, the ratio of initial rotational kinetic energy to initial total kinetic energy is plotted on the horizontal axis and the drag factor is plotted on the vertical axis. The points on this graph show that as the rotational kinetic energy increases as a percentage of the total kinetic energy, the drag factor decreases. The trend line on the graph shows that this decrease occurs parabolically. If one were to ignore the effects of the rotational velocity, and to simply assume that a vehicle with 4 locked wheels would have a drag factor equal to the nominal friction coefficient, regardless of the spin rate, there would be error associated with this assumption even for low rotational kinetic energies. The magnitude of the error would, of course, be larger the larger proportion of the total energy the rotational energy makes up. We leave it to the reader to decide, for any particular case, whether to consider or to ignore the rotational energy, but the results presented here can inform that choice.

In addition to the effects of rotational energy on the deceleration, high yaw velocities can also cause steering angles to develop at the front tires because of the caster angle of the wheel and because the frictional forces between the tires and ground create a torque at the tire contact patch, and cause the yaw rotation of the tires to lag behind the yaw rotation of the vehicle. This too can affect the deceleration and the accuracy of a simulation since it will influence the slip angles at the front tires. In most cases, error introduced by ignoring impact induced steering will be negligible, but if the post-impact yaw velocity is high enough, a simulation can be improved by including it.

References

1. Allen, R., Klyde, D., Rosenthal, T., and Smith, D., "Estimation of Passenger Vehicle Inertial Properties and Their Effect on Stability and Handling," SAE Technical Paper 2003-01-0966, 2003, doi:10.4271/2003-01-0966.
2. Bailey, M., Lawrence, J., Fowler, S., Williamson, P. et al., "Data from Five Staged Car to Car Collisions and Comparison with Simulations," SAE Technical Paper 2000-01-0849, 2000, doi:10.4271/2000-01-0849.
3. Bakker, E., Nyborg, L., and Pacejka, H., "Tyre Modelling for Use in Vehicle Dynamics Studies," SAE Technical Paper 870421, 1987, doi:10.4271/870421.
4. Beauchamp, G., Hessel, D., Rose, N., Fenton, S. et al., "Determining Vehicle Steering and Braking from Yaw Mark Striations," *SAE Int. J. Passeng. Cars - Mech. Syst.* 2(1):291-307, 2009, doi:10.4271/2009-01-0092.
5. Brach, R. and Brach, R., "Modeling Combined Braking and Steering Tire Forces," SAE Technical Paper 2000-01-0357, 2000, doi:10.4271/2000-01-0357.
6. Brach, R. and Brach, M., "Vehicle Accident Analysis and Reconstruction Methods, Second Edition," (Warrendale, SAE International, 2011), doi:10.4271/R-397.
7. Brach, Raymond M., Brach R. Matthew, "Tire Models used in Accident Reconstruction Vehicle Motion Simulation," presented at XVII Europäischen für Unfallforschung und Unfallanalyse (EVU) - Conference, Nice, France, 2008.
8. Brach, R. and Brach, R., "Tire Models for Vehicle Dynamic Simulation and Accident Reconstruction," SAE Technical Paper 2009-01-0102, 2009, doi:10.4271/2009-01-0102.
9. Carter, N., Beauchamp, G., and Rose, N., "Comparison of Calculated Speeds for a Yawing and Braking Vehicle to Full-Scale Vehicle Tests," SAE Technical Paper 2012-01-0620, 2012, doi:10.4271/2012-01-0620.
10. Cliff, W. and Montgomery, D., "Validation of PC-Crash - A Momentum-Based Accident Reconstruction Program," SAE Technical Paper 960885, 1996, doi:10.4271/960885.

11. Cliff, W. and Moser, A., "Reconstruction of Twenty Staged Collisions with PC-Crash's Optimizer," SAE Technical Paper 2001-01-0507, 2001, doi:10.4271/2001-01-0507.
12. Cliff, W., Lawrence, J., Heinrichs, B., and Fricker, T., "Yaw Testing of an Instrumented Vehicle with and without Braking," SAE Technical Paper 2004-01-1187, 2004, doi:10.4271/2004-01-1187.
13. Daily, John, Shigemura, Nathan, Daily, Jeremy, Fundamentals of Traffic Crash Reconstruction, Institute of Police Technology and Management, 2006.
14. Erickson, Mark S., Hayes, Wilson C., "Drag Factor Attenuation for Rotating Vehicles," *Accident Reconstruction Journal*, May/June 2008.
15. Fricke, Lynn B., Traffic Crash Reconstruction, Second Edition, Northwestern University Center for Public Safety, 2010.
16. Martinez, J. and Schlueter, R., "A Primer on the Reconstruction and Presentation of Rollover Accidents," SAE Technical Paper 960647, 1996, doi:10.4271/960647.
17. Steffan, H. and Moser, A., "The Collision and Trajectory Models of PC-CRASH," SAE Technical Paper 960886, 1996, doi:10.4271/960886.

Contact Information

Nathan Rose
Kineticorp, LLC
6070 Greenwood Plaza Blvd., Suite 200
Greenwood Village, Colorado 80111
(303) 733-1888
nrose@kineticorp.com
www.kineticorp.com

The Engineering Meetings Board has approved this paper for publication. It has successfully completed SAE's peer review process under the supervision of the session organizer. The process requires a minimum of three (3) reviews by industry experts.

ISSN 0148-7191

http://papers.sae.org/2016-01-1470